# XMaS

## NEWSLETTER 2024

THE UK MATERIALS SCIENCE BEAMLINE

## CONTENTS



*ON THE COVER:*
*The science portfolio on XMaS embraces a broad range of scientific disciplines some of them being presented in the present Newsletter edition.*

# 30 years ago: birth of XMaS

We are proud to share the diverse and fascinating work of our users in the latest of a long line of XMaS newsletters showcasing the wonderful and inspiring achievements undertaken at our facility. When we started the construction of the beamline back in October 1994, we could never have predicted that we would still be here, stronger than ever with the facility recently passing the 500 papers published benchmark. The ever-broadening scientific scope and excellence continue to inspire us, and we look forward to the milestone of 30 years of operations in 2027.

In this past year we welcomed several visitors to the beamline. In October 2024, Prof Gianluigi Botton, CEO of Diamond Light Source visited. A few weeks later, delegates from the UK Embassy in France, Jeremy Lumb (Head of Science & Innovation, West Europe) and Matthias Meheust-Kemp (Science & Technology Officer) were accompanied by Helen Beadman (Associate Director from STFC Programmes Directorate). The visitors toured the beamline with one of our directors, Yvonne Grunder, who is also the academic member of the British delegation to the ESRF Council. Both visits helped to raise the profile of the facility and the impact of our users' work.

Updates and upgrades have continued to be delivered over the past year, expanding our capabilities and capacities. Our energy dispersive detectors are all operational and available, including the 7-element Ge detector, which finally allows us to exploit the new high energy opportunities. Now both scattering and spectroscopy are available across the entire 2 to 47 keV energy range. Rapid energy changes are possible with minimal re-alignments needed to bring the beam back to the same position. We are also commissioning the KB mirror assembly which gives us a beam ~4 x 6 $\mu m^2$ (H x V) in size with a flux of ~$10^9$ photons/sec. The KB assembly can be rapidly deployed and used to map samples using either scattering or spectroscopy, although it is not yet fully optimised in terms of background or sample alignment procedures. A new gas handling system, designed in collaboration with the Catalysis Hub, will be installed in spring 2025. It allows a range of gases to be delivered to sample environments and, later in 2025, to the ion chambers too. It incorporates a mass spectrometer and will interface directly into the beamline controls. Additional capital improvements have been made possible through the generosity of EPSRC. We can now fully refresh the offline x-ray source and rebuild the low temperature JT cryostat that fits inside the 4 T magnet, regaining our capabilities for sub 10 K operations and increasing the flux of the offline source. New research avenues are being explored in the areas of strain measurements, and we are investing in a new beam position monitor. We will also be able to integrate the Raman system onto the beamline. In terms of software, we will transition from our trusted but obsolete SPEC control to the new ESRF standard, BLISS, which provides greater flexibility in both motor control and data acquisition schemes. Our current macros will need to be translated and tested, which may impact operational access from late 2025 as we commission under operational conditions.

The 10th edition of the XMaS Scientist Experience **[1]** was launched in December 2024 and we look forward to welcoming the winners to the ESRF in July. A new Women in Physics Evening hosted at Warwick **[2]** along with sponsorship of the IoP Conference for Undergraduate Women and Non-Binary Physicists **[3]** focused on undergraduates continues our tradition of supporting outreach focused on the next generation of female scientists.
There have been several changes in the beamline team over the last year. We welcomed the much-needed arrival of Sophie Wawman at Warwick to provide critical administrative and user support. Dr Olga Filimonova moved to a new job on ID26 in September 2024 and we wish her all the very best in her new role. We are pleased to welcome Drs Rachel Kilbride and Florence Legg to the beamline as our new PDRAs noting that they are bringing a wealth of new experience and ideas to the facility.

Finally, please continue to support the facility by applying for beamtime and publishing papers. The next proposal deadline for standard proposals is imminent. We will also be rolling-out our new Block Allocation Group (BAG) in the area of energy materials. We look forward to welcoming you to the beamline and supporting your research activities.

*Chris Lucas, Tom Hase, Yvonne Grunder and Malcolm Cooper*


**[1]** https://warwick.ac.uk/fac/cross_fac/xmas/impact/xmas_scientist_experienceb/
**[2]** https://warwick.ac.uk/fac/cross_fac/xmas/impact/
**[3]** https://www.iop.org/physics-community/cuwip-uk-and-ireland


Fig. 1 (from left to right) Didier Wermeille – XMaS & University of Liverpool, Matthias Meheust-Kemp – Science & Technology Officer, Jeremy Lumb – Head of Science & Innovation West Europe, Helen Beadman – Associate Director from STFC Programmes Directorate and Yvonne Grunder – University of Liverpool.

Grant dates.

2024


Vortex ME4 SSD

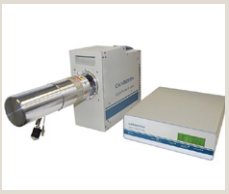

Mirion ME7 HPGe


Raman analyser

2029

2024

Fast scanning monochromator: 2024

2023

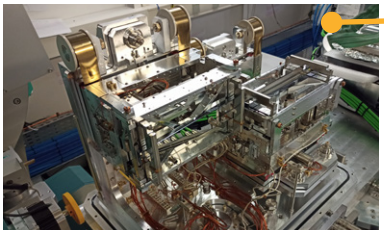

KB mirror

2022

Linkam DSC600

EBS UPGRADE 2019-2020


2020

Pilatus3 S 1M

47 keV: 2020

2019

Lambda 750k CdTe

2017

2015

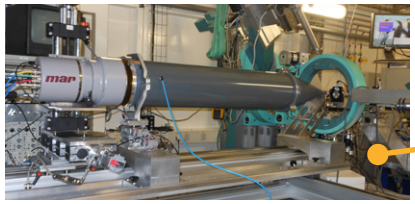

GISAXS rail

X-ray Lab: 2014

Maxipix 2x2

2014

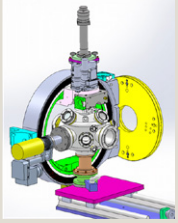

Spectroscopy chamber


Pilatus3 300K

2012

2003


MAR165 CCD

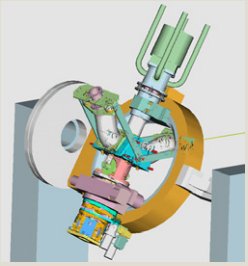

In-vacuum magnet

Electric field capability: 2009

2007

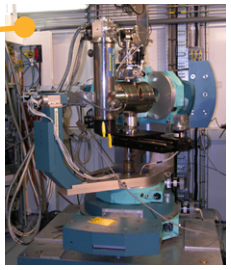

4 T superconducting magnet

2006

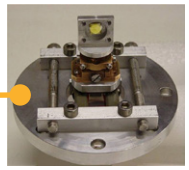

Flipper prototype

2005

2.4 keV: 2004

1 K: 2003

Polarisation analyser

1998

2002

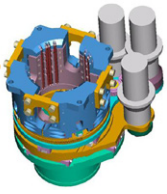

xyz mount

1.7 K: 2001

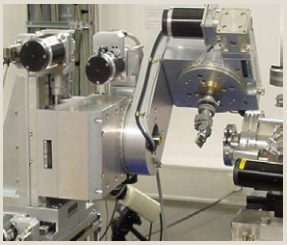

First phase-plate

10-300 K: 1998

FIRST USERS

1997

Diffractometer

FIRST BEAM: 1996

3-15 keV

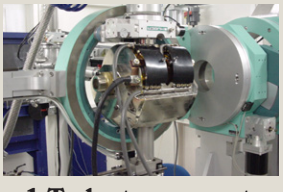

1 T electromagnet

1999

1994

Construction

1996

1991

FIRST DESIGN GRANT

Fig. 2: Project history of the XMaS beamline with milestone achievements and key equipment.

Monochromatic focused beam: 2.035 to 47 keV. 80 µm x 80 µm spot size.
KB microbeam of 5 µm (H) x 7 µm (V) (to be available during late 2025).
Phase-plate crystals to produce circular polarised light between 2.4 and 13 keV.
6-circle Huber diffractometer with double 2θ arm: vertical, horizontal and surface scattering geometries.
In-vacuum polarisation analyser.
High resolution analyser for diffraction.
PE loop system to measure *in-situ* electric polarisation versus electric field in ferroelectric materials.
Impedance analyser.

# TECHNIQUES (individually or in combination)

**Spectroscopy**

- X-ray absorption near edge structure: XANES.
- extended X-ray absorption fine structure: EXAFS.
- (total reflection) X-ray fluorescence: TXRF/XRF.
- grazing incidence X-ray fluorescence: GI-XRF.
- micro X-ray fluorescence: µ-XRF.

**Scattering/Diffraction**

- (surface) X-ray diffraction: SXRD/XRD.
- (grazing incidence) small angle X-ray scattering: (GI)-SAXS.
- (grazing incidence) wide angle X-ray scattering: (GI)-WAXS.
- X-ray reflectivity: XRR.
- resonant magnetic X-ray scattering: RMXS.
- resonant elastic X-ray scattering: REXS.
- powder diffraction: PXRD.

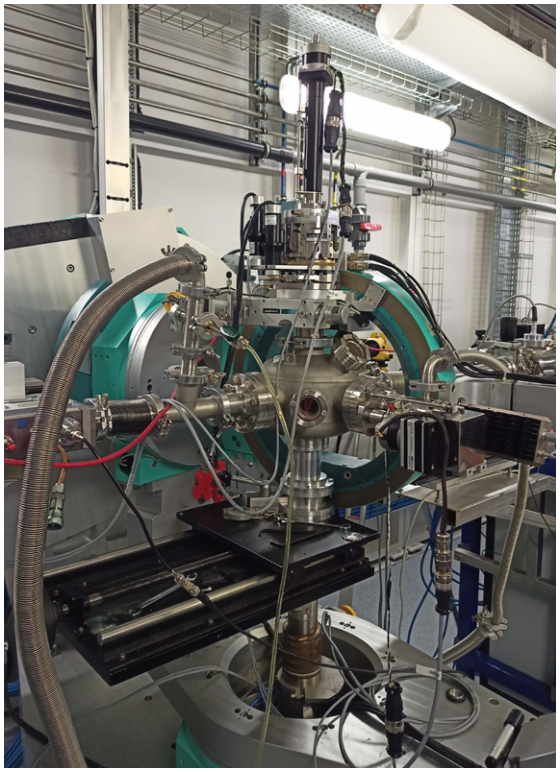

Fig. 3: Low energy fluorescence XANES setup combined with middle and high energy transmission EXAFS.

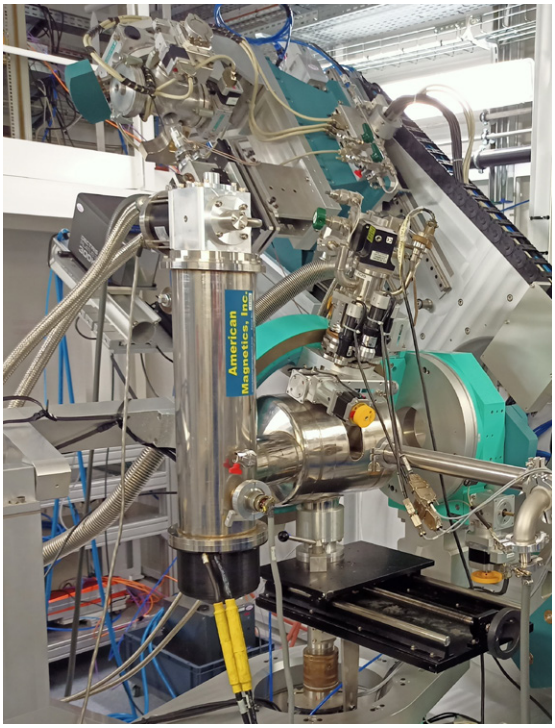


Fig. 4: Low temperature REXS in a 4 T field with polarisation analysis.

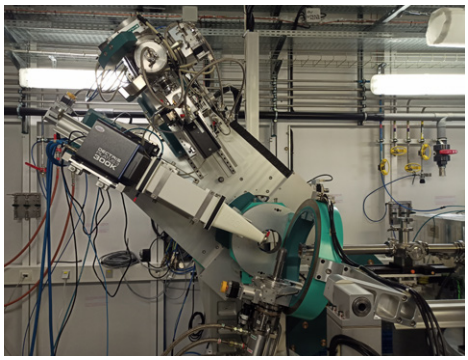

Fig. 5: XRD with a 2D detector and low temperature setup.

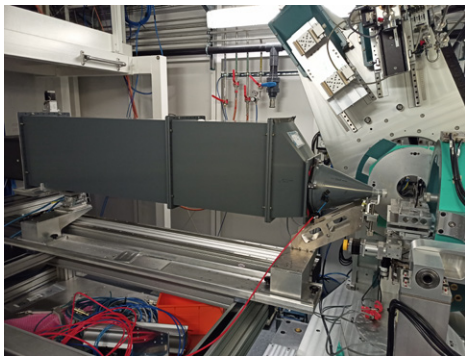

Fig. 6: SAXS setup: new He flight tubes with Pilatus3 S 1M.

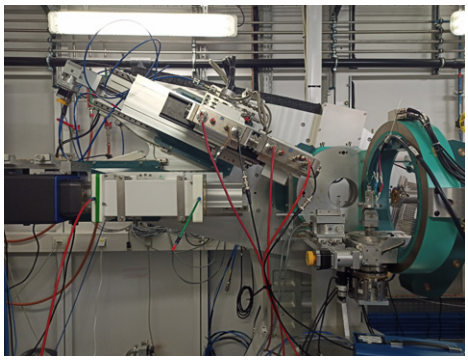

Fig. 7: Combined transmission XANES and EXAFS and high resolution XRD setup.

# DIFFRACTOMETER MOUNTABLE SAMPLE ENVIRONMENTS

**Diverse range of tailorable sample environments for *'in-situ'* and operando studies.**

- Photovoltaic chambers.
- Wet-chemical chamber.
- Electrochemical cell.
- Vacuum/He spectroscopy chamber.
- Gas flow cell.
- Linkam DSC600 calorimetry stage and HFS600-CAP capillary system.
- Cryostats (1.8 K – 700 K) including a system for actinide and transuranic materials.
- Furnace (up to 1000 K, on loan).
- Magnets (±0.1 T up to ±4 T).
- Electric fields (up to 10 kV/mm).

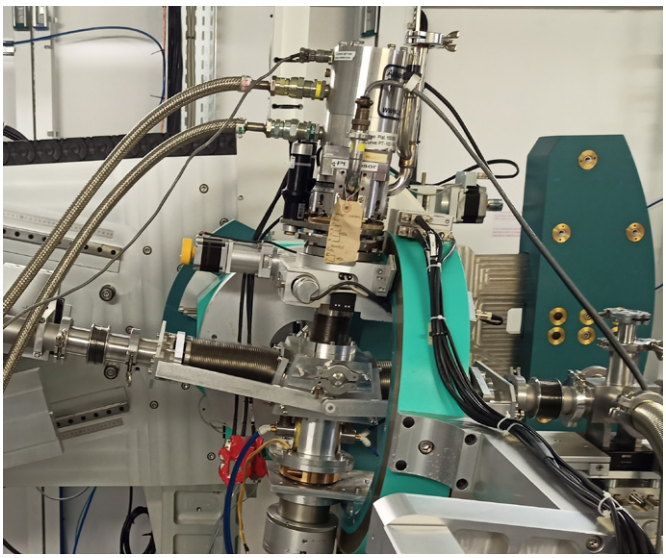

Fig. 8: Low field in-vacuum electromagnet.

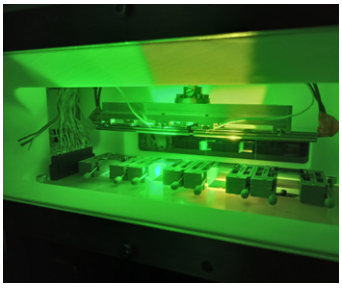

Fig. 9: Photovoltaic chamber with heating capabilities.

Fig. 10: Linkam DSC600 calorimetry stage.

Fig. 11: High voltage amplifier.

Fig. 12: ARS Cryostat.

Custom sample environment can also be adapted to fit on the diffractometer. Please contact a member of the beamline staff to discuss your need.

# DETECTORS

**XMaS offers a wide suite of detectors to exploit the 2.035 - 47 keV X-ray photons and the different X-ray techniques available at the beamline.**

**0D:**

- Ion chambers.
- APD.
- Vortex EX60 0.5 & 2 mm thick SDDs.
- Ketek 150 mm$^2$ 0.5 thick SDD.
- Vortex ME4 2 mm thick SDD.
- Mirion ME7 HPGe.

**2D:**

- Pilatus3 S 1M.
- Pilatus3 300K.
- Maxipix.
- Lambda 750k CdTe.
- MAR165 CCD.


Fig. 13: Vortex ME4 2 mm thick SDD.

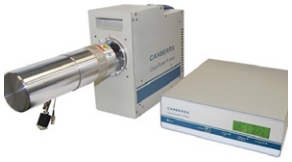

Fig. 14: Mirion ME7 HPGe.


Fig. 15: Pilatus3 300K.


Fig. 16: Pilatus3S 1M.


Fig. 17: Lambda 750k CdTe.


Fig. 18: Maxipix 2x2.

Fig. 19: Vortex EX60 2 mm thick SDD.

# Picometer atomic displacements behind ferroelectricity in the commensurate low-temperature phase of multiferroic $YMn_2O_5$

T. Weigel, C. Richter, M. Nentwich, E. Mehner, V. Garbe, L. Bouchenoire, D. Novikov, D.C. Meyer, M. Zschornak

Multiferroics, which exhibit more than one ferroic property, promise efficient coupling between these properties and present a potential basis for future device applications **[1]**. One of the most intensively studied combination is the coexistence of ferroelectricity (FE) and ferromagnetism providing coupling between electric and magnetic orders.

A notable representative is the manganese-based mullite-phase $YMn_2O_5$, which undergoes multiple phase transitions at low-temperature triggering both magnetism and ferroelectricity **[2]**. In particular, the origin of FE in the commensurate (CM) phase (below $T_{CM}$ = 39 K) has been debated in the past years. It is generally assumed that FE results from changes in the electron density of states, which are magnetically induced by changes in the Mn spin configuration **[3]**.

To date, the CM phase has been described in the non-polar space group *Pbam* (55) that does not allow for FE. Refining the crystal structure in a lower symmetry phase using conventional structure determination has not succeeded due to a lack of sensitivity to shifts of the atomic positions **[2]**. To address this, we used the Resonantly Suppressed Diffraction (RSD) method **[4]** that is very sensitive to structural changes down to the sub-picometer scale. RSD exploits destructive interference of waves diffracted by different atoms that can lead to the suppression of certain Bragg reflections at specific X-ray energies. But the combinations of energy and Bragg reflection are strongly dependent on the precise atomic positions. Measuring the energy-dependence thus gives access to these positions and allowed us to refine the $YMn_2O_5$ structure in both the paraelectric (PE) and ferroelectric (FE) phases, respectively above and below the phase transition temperature $T_{CM}$.

Using the data measured above $T_{CM}$, we refined both the static and dynamic atomic displacements of the PE phase, subsequently improving the model of the FE phase. With this enhanced model, we further refined the static displacements below $T_{CM}$, leading to the first refined structural model of the commensurate phase of $YMn_2O_5$, using the lower-symmetry space group $Pb2_1m$, which allows the polarisation to be along the *b*-direction. Our analysis revealed displacements of the Mn ions and the oxygen structure resulting in a calculated spontaneous polarisation of (1.3 ± 0.4) mC/m², which is close to the measured value of (0.88 ± 0.06) mC/m². We could thus confirm that this electrical polarisation is mainly due to an ionic contribution induced by magnetostriction, confirming that the atomic shifts caused by magnetism lead to the observed ferroelectric behaviour **[5]**.

**[1]** I.H. Lone *et al.*, Nanoscale Res. Lett. 14, 142 (2019).
**[2]** Y. Noda *et al.*, J. Phys. Condens. Matter 20, 434206 (2008).
**[3]** S. Partzsch *et al.*, Phys. Rev. Lett. 107, 057201 (2011).
**[4]** C. Richter *et al.*, Nat. Commun. 9, 178 (2018).
**[5]** T. Weigel *et al.*, Phys. Rev. B 109, 054101 (2024).

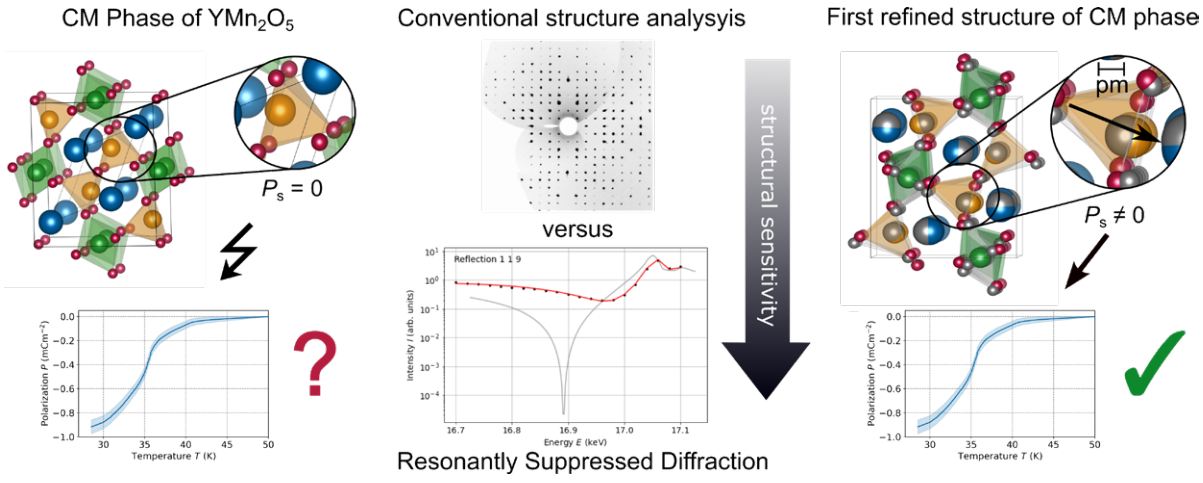


Fig. 20: (left) Ferroelectric CM phase as previously described in the non-polar space group *Pbam*, but that does not allow ferroelectricity. (middle) Refinement in the low-symmetry polar space group $Pb2_1m$ by exploiting the high sensitivity of the RSD method to atomic displacements. (right) Structure of the CM phase exhibiting small displacements of the ions in the pm-range that can explain the measured spontaneous electric polarisation.

**For more information, contact:**

**T. Weigel,**
**Institute of Experimental Physics,**
**Technical University Bergakademie Freiberg,**
**Freiberg, Germany**

**tina.weigel@physik.tu-freiberg.de**

# Phase coexistence and magnetic coupling in $V_2O_3$/Ni heterostructures

K. Ignatova, D. Wermeille, T.P.A. Hase, U.B. Arnalds

Vanadium sesquioxide ($V_2O_3$) is a transition metal oxide which displays remarkable properties including structural, electronic, and magnetic phase transitions. These transitions all occur simultaneously around 150 K and represent a complex, intertwined phenomenon. A particularly intriguing aspect of $V_2O_3$ is the narrow temperature range in which both its monoclinic and rhombohedral phases coexist. The phase transitions and their coexistence are fully reversible with a thermally hysteretic behaviour that can be valuable for technological applications **[1]**.

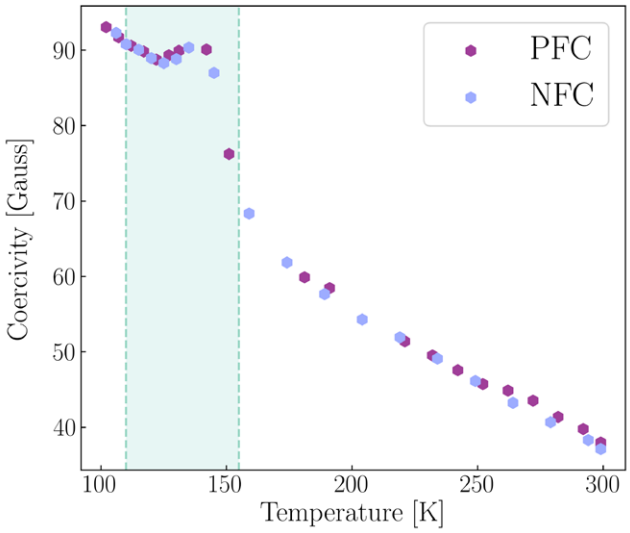


Fig. 22: Coercivity of the $V_2O_3$/Ni film extracted from magnetisation loops recorded using low-temperature MOKE measurements as a function of increasing temperature after positive and negative field cooling (PFC and NFC). A clear peak in coercivity is observed at temperatures coinciding with the phase coexistence region of the $V_2O_3$.

The complex structural evolution of $V_2O_3$ characterised by these phase transitions provides a platform to explore how thin magnetic films such as nickel deposited epitaxially on its surface are influenced by strain **[2]**. This motivated our study on the structural and magnetic properties of a $V_2O_3$/Ni bilayer, which was examined as a function of temperature using high resolution double-axis X-ray diffraction (XRD) and reflectivity measurements. The XMaS 2D detector facilitated the rapid collection and processing of 3-dimensional reciprocal space maps (RSM) **[3]**. These data allow the crystal microstructure of the $V_2O_3$ and the Ni overlayer to be quantified simultaneously across the temperature-driven phase transitions.

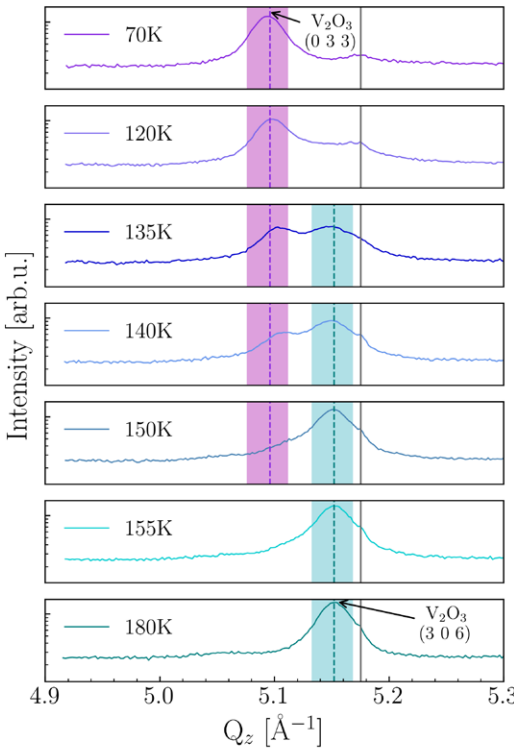


Fig. 21: Temperature-dependent XRD scans recorded along the surface normal for the $V_2O_3$/Ni film as a function of temperature across the structural phase transition of $V_2O_3$. Pink and cyan bars indicate the diffraction peaks for the monoclinic and rhombohedral phases of $V_2O_3$ at low and high temperatures, respectively.

The high-resolution XRD and RSM reveal clearly the structural phase coexistence through the distinct signals coming from the diffraction peaks from the different phases. The temperature spread of the coexistence region spans 110 K to 155 K (see Fig. 21), with the midpoint of the transition at ~130 K. The simple bi-component nature of the mixed phase region induces an increase in the $V_2O_3$ surface roughness observed through temperature-dependent X-ray reflectivity **[3]**. This roughness, which is maximum at the transition midpoint, was found to correlate directly with the magnetic properties of the overlying Ni layer. This was clearly demonstrated by the emergence of a coercivity peak coinciding with the phase coexistence region (see Fig. 22).

Our experiments revealed the direct interplay between structural phase transitions and magnetic properties in hybrid systems, underscoring their potential for functional material design.

**[1]** A. McLeod *et al.*, Nat. Phys. 13, 80 (2017).
**[2]** K. Ignatova *et al.*, J. Condens. Matter Phys. 34, 49 (2022).
**[3]** K. Ignatova *et al.*, APL Mater. 12, 4 (2024).

**For more information, contact:**

**U.B. Arnalds,**
**Science Institute, University of Iceland,**
**Reykjavik, Iceland**

**uarnalds@hi.is**

# The cutting edges of dragons' teeth

A.R.H. LeBlanc, A.P. Morrell, S. Sirovica, O. Addison

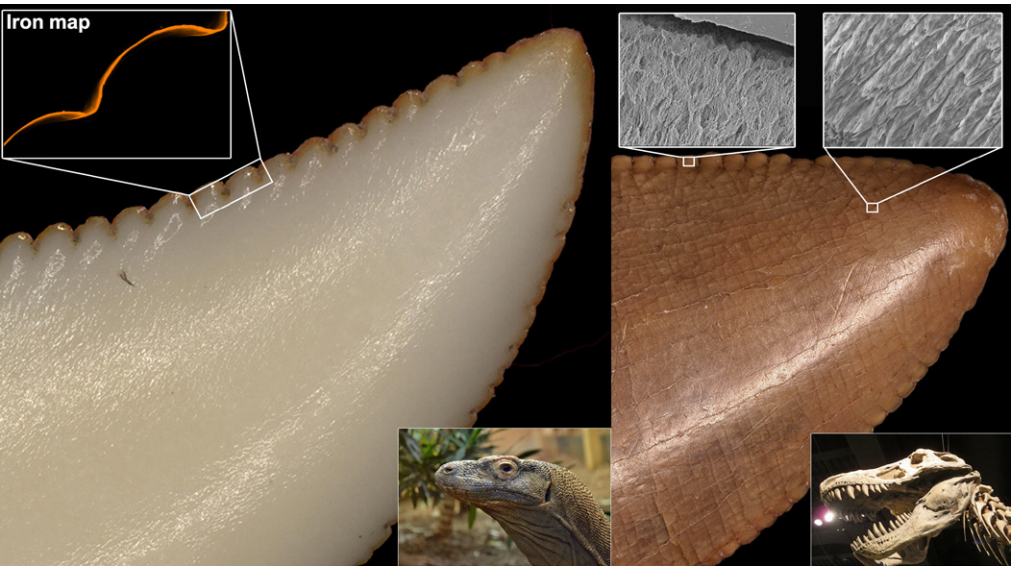


Fig. 23: Comparison of adaptations for maintaining a sharp cutting edge in Komodo dragons (left) and meat-eating dinosaurs (right). Komodo dragon teeth have iron-coated serrations, whereas dinosaurs have different enamel structures on the serrations. Image of Komodo dragon, courtesy of Charlotte Ellis (ZSL).

The Komodo dragons (Varanus komodoensis) of Indonesia have long fascinated scientists. As the largest living lizards, they are able to hunt prey much larger than themselves and use a mouth lined with serrated, blade-shaped teeth to subdue their prey. They also make excellent models for understanding how extinct animals with similarly blade-shaped teeth – like meat-eating dinosaurs – might have used them to hunt. But how well do we really know our living model?

Our recent research **[1,2]** investigated the cutting prowess of Komodo dragon teeth using state-of-the-art techniques at the ESRF to look at the chemistry and structure of the thin veneer of enamel coating their teeth. We then compared these with a sample of alligator and crocodile teeth, and finally to a sample of fossil meat-eating dinosaur teeth from the Cretaceous period of Western Canada.

What we discovered was surprising. Komodo dragons have evolved a special iron-rich coating along the serrated edges of each of their teeth (Fig. 23). This coating, rich in iron oxides that stain the cutting edges and tooth tips orange, protects these parts of each tooth from wearing too quickly, thus maintaining a sharp cutting edge. Iron-enriched enamel is a feature we classically associate with mammal teeth (e.g. rats, beavers, and shrews), but not the teeth of lizards or other reptiles.

This finding led us to look more closely at the teeth of alligators and crocodiles: reptiles that lack the blade-like teeth of Komodo dragons, but have sharp cutting edges to their teeth. Here too we discovered iron-enriched enamel along the cutting edges, but to a lesser degree than in Komodo dragons. This suggested to us that iron-coated teeth may be more widespread among reptiles. Could the serrations of meat-eating dinosaur teeth harbour the same adaptations?

Unfortunately, as one of the most common elements on the Earth's surface, iron has seeped into all of the inner parts of dinosaur teeth. This makes it difficult to determine if dinosaurs were similarly able to reinforce their serrated teeth with iron in life. However, using advanced structural imaging techniques at XMaS/BM28, we showed a different, but equally impressive adaptation hidden within the teeth of meat-eating dinosaurs.

Whereas Komodo dragons have altered the chemistry of their teeth, meat-eating dinosaurs changed the structure of the enamel along their serrations. The enamel of each dinosaur serration forms tight spirals of mineral crystals, imparting a higher resistance to tooth wear along the cutting edges of their teeth compared with the more regular enamel structure found elsewhere on each tooth (Fig. 23).

These findings demonstrated that, while their teeth may look similar on the outside, meat-eating reptiles can evolve different and unexpected ways of maintaining a cutting edge.

**[1]** A.R.H. LeBlanc *et al.*, Nat. Ecol. Evol. 8, 1711 (2024).
**[2]** Project funded by the European Research Council's Horizon 2020 programme (no. 894331).

**For more information, contact:**

**A.R.H. LeBlanc,**
**Faculty of Dentistry,**
**Oral & Craniofacial Sciences,**
**King's College London, UK**

**aaron.leblanc@kcl.ac.uk**

# The surprising chemistry of arsenic and mixed-valent iron minerals

J. Biswakarma, M. Matthews, J.M. Byrne

Arsenic contamination in groundwater is one of the most pressing environmental and public health challenges, particularly in regions of the Global South such as Southeast and Central Asia and South America. Millions of people depend on groundwater in these areas for drinking and irrigation. Yet many water sources exceed safe arsenic limits. Long-term exposure to arsenic can lead to severe health consequences, including skin lesions, cardiovascular diseases, and developmental issues.

Arsenic primarily exists in two forms in natural environments: arsenite (As(III)) and arsenate (As(V)). As(III) is significantly more toxic and mobile, posing a serious threat to groundwater quality. Until now, it has been widely believed that As(III) could only be oxidised to As(V) in oxygen-rich environments. We challenged this concept by conducting sorption experiments with As(III) on green rust sulfate (GR-$SO_4$), a mixed-valent iron (oxyhydr)oxide mineral, under pH-neutral, anoxic conditions, both with and without citrate, a plant exudate.

As shown in Fig. 24, our As K-edge study showed that As(III) sorbed to green rust sulfate was partially oxidised under reducing conditions and completely oxidised in the presence of citrate at pH 7.0. Meanwhile, the Fe K-edge analysis revealed that green rust sulfate underwent a phase transformation to another iron mineral, generating labile Fe(III), which facilitated As(III) oxidation.

These findings **[1]** not only challenge the idea that arsenic oxidation requires oxygen but also highlight the role of naturally occurring mixed-valent iron minerals in this transformation. Green rust sulfate, in particular, acts as a sink for arsenic by promoting the oxidation of toxic As(III) to the less mobile As(V). This process could help explain the behaviour of arsenic in natural environments and its reduced mobility in certain groundwater systems.

Our study also highlights the role of organic matter in this process. Organic ligands, such as citrate, commonly found in soils and groundwater, stabilise iron species and significantly enhance the oxidation of As(III) to As(V). These findings suggest that natural processes involving mixed phases of iron minerals and organic matter play a critical role in controlling arsenic mobility and toxicity in real-world environments.

Understanding these processes is essential for developing sustainable management and treatment strategies for arsenic contaminated groundwater.

**[1]** J. Biswakarma *et al.*, Environ. Sci. Technol. Lett. 11, 1239 (2024).

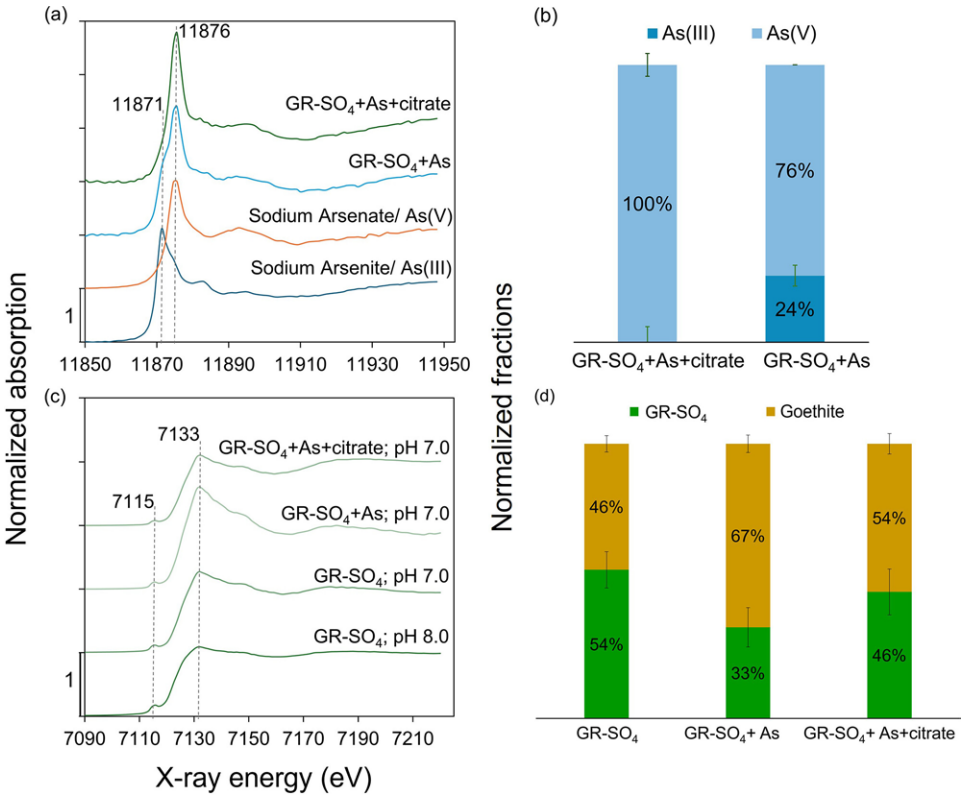


Fig. 24: XANES at As K-edge (a) and Fe K-edge (c) of solid samples collected before and after As(III) sorption experiments. The 1 g $L^{-1}$ GR-$SO_4$ suspension was exposed to As(III) (500 µg $L^{-1}$) in the presence and absence of citrate (50 µM) at pH 7.0 under anoxic conditions. Calculated Linear Combination Fitting (LCF) fractions of XANES data presented for As speciation (b) and different Fe phases (d).

**For more information, contact:**

**J. Biswakarma,**
**School of Earth Sciences,**
**University of Bristol, UK.**

**jagannath.biswakarma@bristol.ac.uk**

# Coating nanocrystals an atomic layer at a time

P.B. Green, O. Segura Lecina, P.P. Albertini, M.A. Newton, K. Kumar, C. Boulanger, J. Leemans, P.B.J. Thompson, A. Loiudice, R. Buonsanti

Atomic layer deposition (ALD) is a method to grow thin coatings on materials one single atomic layer at a time **[1]**. This approach has been employed in applications ranging from catalysis to optoelectronics. ALD is a gas phase technique and thus, is incompatible with colloidal materials such as nanocrystals (NCs). NCs stand to greatly benefit from combining protective coatings grown by ALD and their inherent solution processability. Such a protocol could pave the way to more stable NC based catalysts and LEDs **[2,3]**. Our aim was then to develop a new colloidal ALD (c-ALD) method that preserves the properties of NCs while endowing the advantages of ALD **[4]**.

To this end, we devised c-ALD herein to grow metal oxides on a variety of nanocrystalline composition. Our scheme relies on precise knowledge of the NC surface chemistry. Through in-depth solution nuclear magnetic resonance (NMR) studies, we found that metal amides reacted in a self-limiting way with the native carboxylate passivated surfaces of our NCs, resulting in a monolayer thick coating. Key to the process was the use of ligand modified metal amides as the metal precursor and oleic acid as the oxygen precursor (Fig. 25A). Both precursors are excellent colloidal stabilising ligands, which thus did not compromise the colloidal stability of the NCs upon growth of the coatings.

To characterise the grown coatings, we went to XMaS/BM28 that offered an exciting combination of techniques, namely high-resolution X-ray diffraction (XRD) and X-ray absorption spectroscopy (XAS). XRD was employed to pin down any changes to the crystalline structure of the NCs or the metal oxide upon growth of the coatings. XAS was used to track the structural evolution of the grown coatings as more c-ALD cycles were performed (Fig. 25B-C) **[4]**. Through this insight we could design better coatings.

Our next goal is to develop this protocol further and to study the properties of the coated NC based photo- and electrocatalyst under harsh chemical reaction conditions.

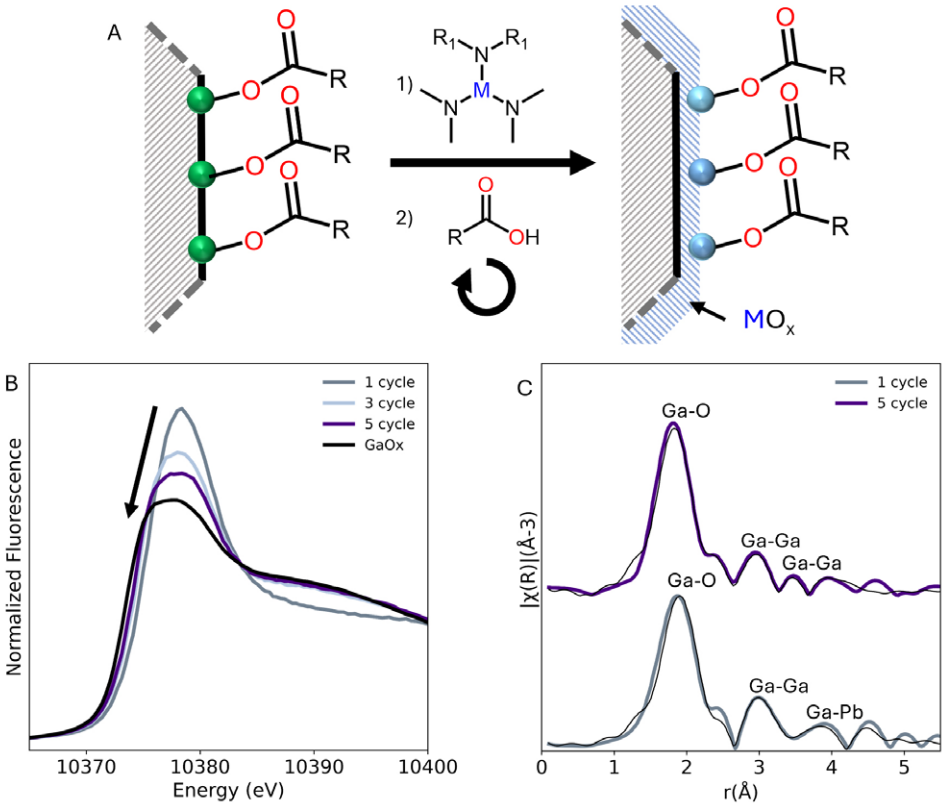


Fig. 25: (A) Scheme of the developed c-ALD protocol: using metal amides and carboxylic acids a variety of metal oxides could be grown by c-ALD on carboxylate passivated NCs. (B) Ga K-edge XANES of PbS NCs having undergone a few cycles of c-ALD to grow gallium oxide. (C) Fourier transform of the Ga K-edge EXAFS for the same samples shown in (B) and their respective fits (black lines). XAS allowed us to track the evolution of the grown coatings.

**[1]** R.W. Johnson *et al.*, Mater. Today 17, 5, 236 (2014).
**[2]** P.P. Albertini *et al.*, Nat. Mater. 23, 680 (2024).
**[3]** O. Segura Lecina *et al.*, JACS Au 3, 11, 3066 (2023).
**[4]** P.B. Green *et al.*, J. Am. Chem. Soc. 146, 15, 10708 (2024).

**For more information, contact:**

**R. Buonsanti,**
**Institute of Chemical Science and Engineering, École Polytechnique Fédérale de Lausanne, CH.**

**Raffaella.buonsanti@epfl.ch**

# Investigating the strain-induced crystallisation behaviour of self-healing natural rubber vulcanisates

E.L. Heeley, D.J. Hughes, A.M. Wemyss, A. Little, E.M. Crabb, C. Wan

Vulcanised natural rubber (NR), used in vehicle tyres, has excellent resilience and mechanical properties e.g. tensile strength, elasticity and tear resistance. The mechanical properties of NR are linked to the molecular orientation and strain-induced crystallisation (SIC) behaviour of its 3D covalent network structure. Yet, this structure inhibits NR from being reprocessed or recycled. Developing a new generation of vulcanised rubbers with balanced mechanical strength and self-healing properties is therefore vital. To address this challenge, we have developed a set of self-healing rubber-carbon black (NR/CB) composites having comparable mechanical properties to NR. In this investigation four NR composites with 40 parts per hundred CB particles with size of N660 > N330 > N234 > N135 were prepared.

To investigate the SIC behaviour of these NR/CB composites combined 2D wide-angle X-ray scattering (WAXS) and tensile testing measurements were performed on XMaS/BM28 **[1]**. WAXS of the NR/CB composites was monitored *in-situ* at **25°C** and mapped on to the tensile testing curves. Fig. 26A shows the stress-strain curves (up to 400% strain) for the NR/CB composites and control NR sample without CB filler. The addition of CB has a reinforcing effect on the mechanical properties of NR. The upturn of the stress in all NR/CB composites occurs at lower stress compared with the unfilled rubber, where the NR/330 composite exhibits the greatest difference in reinforcement.

Clear oriented crystalline peaks indexed as the (200), (201) and (120) appeared in the WAXS pattern measured in the NR/330 composite at a final strain of 400% (Fig. 26B) in contrast with NR, which shows little crystalline peak development at the same strain value.

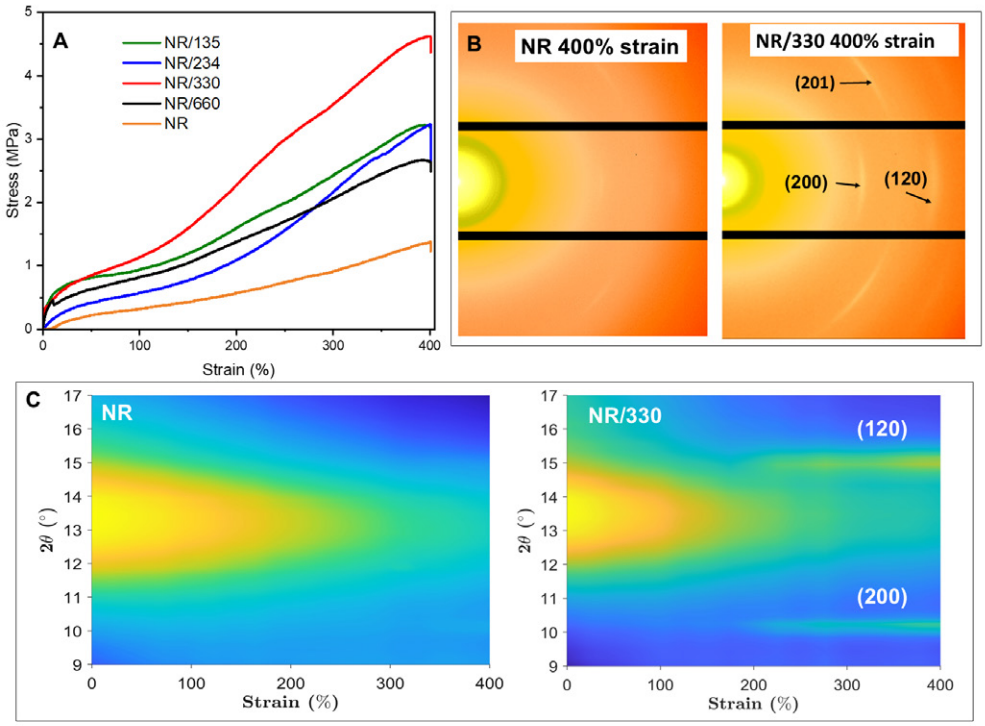


Fig. 26: (A) Stress-strain curves; (B) 2D WAXS patterns of NR and NR/330 at 400% strain; (C) WAXS surface plots during the drawing of NR and NR/330.

Fig. 26C shows the surface plots of the equatorial scattering intensity for NR/330 composite and NR from 0% to 400% strain. The development of the (120) and (200) peaks indicates the onset of crystallisation in the NR/330 composite at ~200% strain, but these peaks are not observed in the NR sample. Therefore, SIC occurs at lower strains in the NR/CB composites compared to unfilled NR, indicating that the CB filler enhances SIC in this strain region.

Here, we have demonstrated that the addition of CB filler in NR not only has a reinforcing effect on the mechanical properties, but SIC commences at lower strains compared with the unfilled NR.

**[1]** T. Xia *et al.*, ACS Sustainable Chem. Eng. 11, 50, 17857 (2023).

**For more information, contact:**

**E.L. Heeley,**
**School of Life,**
**Health and Chemical Sciences,**
**The Open University, U.K.**

**Ellen.Heeley@open.ac.uk**

# Investigating the generation of free charges in organic solar cells

A. Jungbluth, M. Riede

Organic solar cells (OSC) have made significant progress in recent years and their unique advantages – weighing much less than conventional solar cells, being mechanically flexible, and offering optional semitransparency – open massive new markets for harnessing the power of the sun **[1]**.

However, power conversion efficien-cies (PCE) need to be improved further to accelerate the roll-out of OSC. Thus, this study investigates the factors limiting charge generation in OSCs with low energy offsets between donor and acceptor molecules, something that is desired for high-efficiency OSC. The researchers focused on vacuum-processed fullerene-based OSCs, which have struggled to achieve the high performance seen in some non-fullerene acceptor (NFA) systems with similarly low offsets, while being more production relevant.

The international and inter-disciplinary team from the University of Bern, Florence and Oxford as well at Georgia Tech, DGIST in Korea, Diamond Light Source and XMaS/BM28 examined blends of zinc phthalocyanine (ZnPc) molecules with varying levels of fluorination (F0, F4, F8, F16) as donors at 5 wt% and C60 as the acceptor at 95 wt% **[2]**. Fluorination gradually shifts the energy levels of the donor molecules while the dilute nature keeps the blend microstructure comparable between all samples, allowing to selectively study how different energy offsets affect device performance **[3]**.

As fluorination increased, the open-circuit voltage of the solar cells improved but the short-circuit current decreased significantly. The ZnPc and F4ZnPc blends showed efficient charge generation, while F8ZnPc and F16ZnPc blends had severely limited photocurrents.

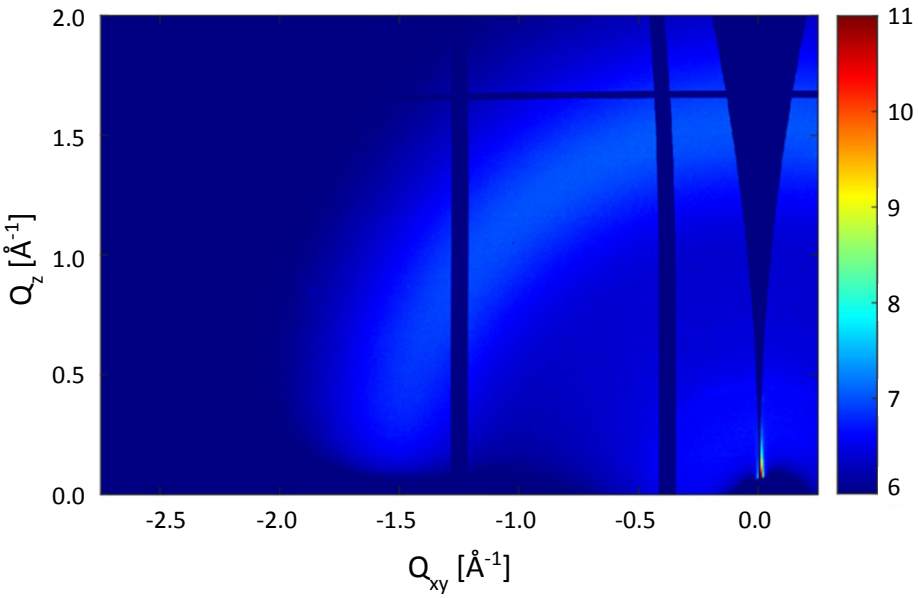


Fig. 27: Grazing incidence wide-angle X-ray scattering (GIWAXS) reciprocal space maps of the dilute F4ZnPc:C60 blend, measured at XMaS and proving comparable micro-structure to all other dilute blends.

Digging deeper, the research team used various spectroscopic techniques combined with DFT calculations to investigate the charge transfer (CT) and charge separation (CS) processes in these blends. For ZnPc and F4ZnPc blends, CT state formation and dissociation were efficient, leading to good device performance. In F8ZnPc blends, CT state formation was still relatively efficient, but CT state dissociation became a major bottleneck, limiting free charge generation. For F16ZnPc blends, both CT state formation and CS were limited, resulting in poor performance.

The study highlights that the transition from CT states to CS states can be a critical limiting factor in low-offset fullerene-based OSCs. This challenges the common understanding that CT state formation is the primary limiting factor in these systems.

This work suggest that the success of some NFA systems with low offsets may be due to more efficient CT-CS transitions, rather than just efficient CT state formation and emphasises the need to consider both the energetics of CT state formation and the dynamics of charge separation when designing and optimising OSC materials. It also demonstrates the value of using model systems with systematically varied properties to unravel complex photo-physical processes in these devices. Understanding these fundamental processes is crucial for the continued development of OSC as a promising renewable energy technology.

**[1]** J.C. Blakesley *et al.*, J. Phys. Energy 6, 041501 (2024).
**[2]** A. Jungbluth *et al.*, Nat. Comm. 15, 5488 (2024).
**[3]** M. Schwarze *et al.*, Nat. Comm. 10, 2466 (2019).

**For more information, contact:**

**M. Riede,**
**Department of Physics,**
**University of Oxford, UK.**

**moritz.riede@physics.ox.ac.uk**

# Revolutionising solar energy: super stable perovskite coatings

F. Yang, Y.-H. Lin, H. Snaith

Imagine a future where everyday objects – backpacks, cars and mobile phones – generate electricity from sunlight. This vision is closer than ever thanks to perovskite solar cells: ultra-thin, flexible coatings that seamlessly integrate into surfaces. At just over one micron thick, they offer a sustainable alternative to bulky silicon solar panels, reducing reliance on large solar farms and preserving valuable farmland for food production. With solar energy now 90% cheaper than it was 14 years ago, this innovative technology could transform renewable energy into the most practical and accessible solution for a sustainable future **[1]**.

Despite their remarkable efficiency and affordability, perovskite solar cells face challenges with long-term stability. In this study, we developed a vapor-based amino-silane treatment to address these issues, reducing energy losses to just 100 millivolts – over 90% of the theoretical efficiency limit – for materials with energy bandgaps between 1.6 and 1.8 electron volts, which are critical for tandem solar cells **[2]**.

Amino-silane molecules with both primary and secondary amine groups significantly enhanced light emission by up to 60 times while maintaining excellent charge conduction. Devices treated with these molecules retained 95% of their efficiency for over 1,500 hours under harsh conditions, including continuous sunlight at 85°C and high humidity.

To investigate the mechanism behind this improvement, we conducted grazing incidence wide angle X-ray scattering (GIWAXS) on XMaS/BM28 **[2]**. These experiments revealed that primary amine molecules like APTMS induced a solvation process in perovskite films, breaking down the crystalline structure into a modified but well-passivated form. This transformation made the films hazier and more transparent while preserving strong light absorption and photoluminescence (Fig. 28).

In contrast, secondary amine molecules like AEAPTMS created a stable surface layer without disrupting the bulk perovskite structure. The GIWAXS measurements showed that AEAPTMS-treated films maintained their crystallinity, with X-ray signals weakening only due to the accumulation of surface molecules. These findings demonstrate how different amino-silane molecules interact uniquely with perovskite materials, offering valuable insights into optimising treatments for enhanced performance and durability.

By advancing the stability and efficiency of perovskite solar cells, this work brings us closer to a future powered by seamlessly integrated, sustainable solar energy.

**[1]** D. Connett, "Solar energy breakthrough could mean solar panels will be a thing of the past", The I paper, https://inews.co.uk/news/business/solar-energy-breakthrough-solar-panels-oxford-university-3219693.
**[2]** Y.-H. Lin *et al.*, Science 384, 767 (2024).

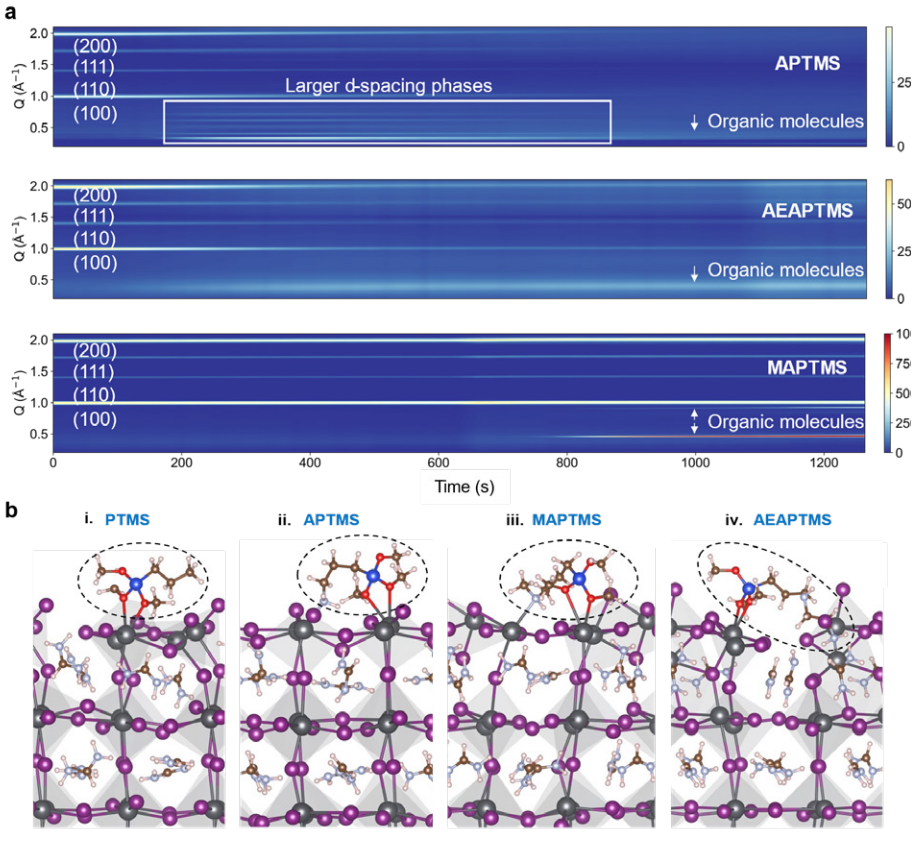


Fig. 28: Structural analysis of the amino-silane-surface interactions: (a) Time-dependent GIWAXS patterns measured at incident angles of 1° for the vapour-based depositions of APTMS (top), AEAPTMS (middle), and MAPTMS (bottom) on I0.9Br0.1 perovskite films, with the background signals from air scattering, Kapton-taped window, glass, and ITO removed. The slight tilt observed in all the signals acquired with time is due to the thermal extension of the sample stage, which causes a partial loss of alignment. (b) Simulated structures using DFT and AIMD techniques of the interactions of the amino-silanes PTMS, APTMS, MAPTMS and AEAPTMS with the Pb/I terminated (001) FAPbI3 surface. PbI6 octahedra are highlighted to show that the major structural relaxation is found mostly in the uppermost layer.

**For more information, contact:**

**Y.-H. Lin,**
**Department of Electronic and Computer Engineering,**
**The Hong Kong University of Science and Technology, Hong Kong SAR.**

**yh.lin@ust.hk**

# Covalently bound iron porphyrin functionalised carbon nanotubes for oxygen reduction reaction

Q. Li, Y. Xu, A. Pedersen, M. Wang, M. Zhang, J. Feng, H.Luo, M.-M. Titirici and C. R. Jones

The oxygen reduction reaction (ORR) is a critical process in energy conversion technologies such as alkaline exchange membrane fuel cells and metal-air batteries. Iron triphenyl-porphyrin (FeTPP), with a well-defined Fe-$N_4$ configuration, has been extensively utilised as an ORR electrocatalyst to advance the understanding of the reaction mechanism. However, an overlooked yet significant factor in this system is the functionalisation method and its impact on the interaction between the catalyst molecule and the carbon support during the ORR process.

This work focused on two methods of attaching FeTPP molecules to carbon nanotubes (CNTs): covalent bonding and non-covalent attachment. The covalent approach uses the aryl diazonium reaction to form a robust C-C bond between iron porphyrin and the CNTs (Fig. 29). In the non-covalent method, molecules are mixed with CNTs, relying on physical interactions.

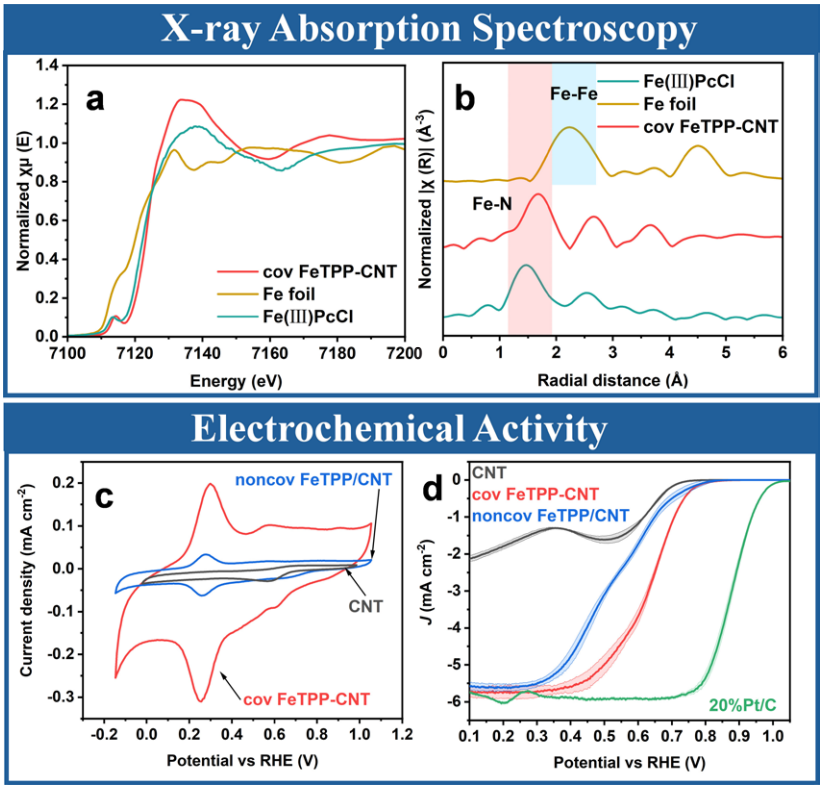


Fig. 30: (a) Fe K-edge XANES spectra and (b) Fourier transform EXAFS of cov FeTPP-CNT, Fe foil, and Fe (III)PcCl; (c) cyclic voltammetry in $N_2$ and (d) Linear sweep voltammetry in $O_2$ of catalysts.

Using X-ray absorption spectroscopy (XAS) at XMaS/BM28, the local atomistic and electronic structure of Fe in the covalently functionalised FeTPP-CNT (cov FeTPP-CNT) sample could be examined (Fig. 30 a-b). The *ex-situ* X-ray absorption near edge structure (XANES) spectra collected at the Fe K-edge confirmed the $Fe^{3+}$ oxidation state in the cov FeTPP-CNT catalyst. Additionally, the small peak is also observed at about 7114 eV in both FeTPP-CNT and Fe (III)Pc-Cl, suggesting a distorted square planar geometry which is possibly caused by the axial Cl− group on the FeTPP. Fourier transformed extended X-ray absorption fine structure (EXAFS) further reveals the presence of the Fe—N bond in the first shell of the cov FeTPP-CNT, indicating that the majority of the Fe species in the sample exist as isolated single atoms.

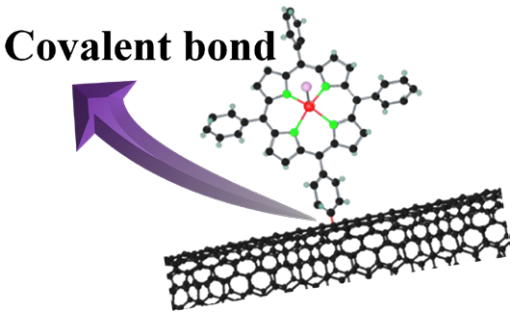


Fig. 29: Structure of Cov FeTPP-CNT.

The cov FeTPP-CNT catalyst exhibited six times the number of active catalytic sites density (estimated by integrating the peak area of Fe shown in Fig.30c) and superior electrochemical active site utilisation of 12.7%, compared to 2.8% observed for the non-covalent sample (noncov FeTPP/CNT). These results demonstrate that the covalent approach effectively addresses the issue of molecular aggregation, enabling a more uniform distribution on the CNT support. Further, ORR tests revealed the covalent functional methods could improve the ORR activity, as depicted in Fig. 30d, and promote a more favourable 4-electron pathway. These insights into the functionalisation method are valuable for the design of catalysts with high active site density and improved performance.

**[1]** Q. Li *et al.*, Adv. Funct. Mater. 34, 2311086, (2024).

**For more information, contact:**

**Q. Li,**
**Department of Chemistry,**
**Queen Mary University of London, UK**

**qi.li@qmul.ac.uk**

# ACCESS TO SYNCHROTRON and OFFLINE FACILITIES

Two proposal review rounds are held each year. Deadlines for applications to make use of the National Research Facility (CRG) time are normally 1st April and 1st October for the scheduling periods August to February and March to July, respectively.

Applications for beamtime must be submitted electronically via the ESRF web page: **www.esrf.eu**. Select **"Users & Science"**, then choose **"Applying for beamtime"** from the drop-down list. On the right hand side, you can consult the instructions to submit your proposal and access the **"User Portal"**. Enter your surname and password and select **"Proposals/Experiments"**. Follow the instructions carefully — you must choose **"Collaborative Research Group"** and **"BM28 (XMaS) UK Materials Science CRG Beamline"** at the appropriate stage in the process. If you experience any problems, please contact Laurence Bouchenoire (**bouchenoire@esrf.fr**). Technical specifications and instrumentation available are described on the XMaS web page (**www.xmas.ac.uk**). All sections of the form must be filled in. Particular attention should be given to the safety aspects with the name and characteristics of your samples completed carefully. Experiments requiring special safety precautions such as the use of electric fields, lasers, high pressure cells, dangerous substances, toxic substances and radioactive materials, must be stated clearly in the proposal. Moreover, any ancillary equipment supplied by the user must conform to the appropriate French regulations. Further information may be obtained from Martine Moroni, the ESRF Experimental Safety Officer for CRG beamlines (**martine.moroni@esrf.fr**, tel: +33 4 76 88 23 69). Please indicate your date preferences, including any dates that you would be unable to attend if invited for an experiment. This will help us to produce a schedule that is satisfactory for all.

When preparing your application, please consider that access to the National Research Facility is reserved for UK based researchers. Collaborations with EU and international colleagues are encouraged, but the proposal must be led by a UK based principal investigator. It must be made clear how any collaborative research supports the wider UK science base. Applications without a robust link to the UK will be rejected and should instead be submitted directly to the ESRF using their public access route.

Access to the XMaS beamline is also available for one third of its operational time to the ESRF's user community. Applications for beamtime within that quota should be made in the **ESRF's proposal rounds (application deadlines 3rd March and 10th September**). Applications for the same experiment may be made to both XMaS directly and to the ESRF. Obviously, proposals successfully awarded beamtime by the ESRF will not then be given additional time in the XMaS allocation.

An experimental report on completed experiments must be submitted electronically, following the ESRF model. The procedure for submitting experimental reports follows that for the submission of proposals. Please follow the instructions on the ESRF's web pages carefully. **Reports must be submitted within 3 months of the experiment**. Note that the abstract of a publication can also serve as the experimental report! Please also remember to fill in the XMaS end of run survey form on completion of your experiment, which is available on the website (**https://bit.ly/3JM6E7q**).

### Assessment of Applications

The independent Peer Review Panel considers the proposals, grades them according to scientific excellence, adjusts the requested beam time if required, and recommends proposals to be allocated beam time on the beamline. Experimental reports will also form part of the assessment criterion. Proposals which are allocated beamtime must meet ESRF safety and XMaS technical feasibility requirements. Following each meeting of the Peer Review Panel, proposers will be informed of the decisions taken and feedback provided.

## APPLICATIONS FOR OFFLINE FACILITY TIME

Submit your application directly on the XMaS web site: **www.xmas.ac.uk**. Select **"XMaS Offline Facilities"** and then **"Application for Offline Facilities"**. Follow the instructions carefully and do not forget to upload your 1-2 page proposal at the end of the application form. Please contact the local staff to discuss any potential experiments. Successful offline proposals will be run as in-house experiments. We will complete the safety form with the information supplied in your application form as well as arrange site passes and any accommodation that may be required. As for synchrotron beamtime, offline users normally stay in the ESRF guest house or off-site hotels.

*The XMaS facility implements transparent policies and procedures to guarantee that access is based on scientific excellence only. In partnership with the ESRF Safety office, we will endeavor to ensure that the facility can accommodate any user, but this may require an individual needs assessment. If you have any questions about accessing the facility at any stage of the application or experimental processes, please do not hesitate to get in touch.*

### Living allowances

These are €90 per day per beamline user — the equivalent actually reimbursed in sterling. XMaS will support up to 3 users per synchrotron experiment and only 1 on the offline laboratories. For experiments which are user intensive, additional support may be available. The ESRF hostel still appears adequate to accommodate all our users, though CRG users will always have a lower priority than the ESRF's own users. Do remember to complete the "A-form" when requested to by the ESRF, as this is used for hostel bookings, site passes and to inform the safety group of attendees.

# Beamline people

**Didier Wermeille**
didier.wermeille@esrf.fr
is the Beamline Responsible who, in partnership with the Directors, oversees the activities of the user communities as well as the programmes and developments that are performed on the beamline. He is also the beamline Safety Representative. His expertise spans crystallography, high resolution diffraction, surface studies, magnetic scattering and electric field measurements.

**Laurence Bouchenoire**
bouchenoire@esrf.fr is the Beamline Coordinator. She looks after beamline operations and can provide you with information about the beamline, application procedures, scheduling, etc. Laurence should normally be your first point of contact. Her expertise is in magnetic scattering including polarisation dependence.

**Oier Bikondoa**
oier.bikondoa@esrf.fr
is Beamline Scientist with expertise in soft matter materials, (GI-)SAXS/WAXS, surface and reflectivity studies.

**Paul Thompson**
pthompso@esrf.fr
is the contact for instrument development, technical support, sample environments including electric field, liquid cells and catalysis.

## PROJECT DIRECTORS

**Chris Lucas** clucas@liv.ac.uk

**Tom Hase** t.p.a.hase@warwick.ac.uk

and **Yvonne Grunder**
yvonne.grunder@liverpool.ac.uk
continue to travel between the UK and France to oversee the operation of the beamline.

**Malcolm Cooper**
m.j.cooper@warwick.ac.uk
remains involved in the beamline operation as an Emeritus Professor at the University of Warwick.

## PROJECT ADMINISTRATORS

**Sophie Wawman**
Sophie.Wawman@warwick.ac.uk

and **Julie Clark**
Julie.Clark@liverpool.ac.uk
are the administrators on the project, based in the Department of Physics at Warwick and Liverpool, respectively. Sophie is the point of contact for user T&S claims and co-ordinates the annual XMaS Scientist Experience.

## THE PROJECT MANAGEMENT COMMITTEE

The current membership of the committee is as follows:
**C. Nicklin (chair)**, DLS
**L. Behrooz,** EPSRC
**M. Alfredsson,** Uni. of Kent
**M. Cain,** Electrosciences Ltd
**A. Beale,** Uni. College London
**K. Edler,** Uni. of Bath
**S. Langridge,** ISIS

In addition to the above, the directors, the chair of the Peer Review Panel, the CRG Liaison T. Buslaps and the beamline team are in attendance at the meetings which happen twice a year.

## THE PEER REVIEW PANEL

The current membership of the panel is as follows:
**R. Arrigo (chair),** Uni. of Salford
**A. Hector,** Uni. of Southampton
**E. Heeley,** Open University
**M. Skoda,** ISIS
**K. Syres,** Uni. of Central Lancashire
**L. Ishibe-Veiga,** DLS
**M. Senn,** Uni. of Warwick.

In addition, either Chris Lucas, Yvonne Grunder or Tom Hase attends their meetings in an advisory role.

## PUBLISH PLEASE!!... and keep us informed

One of the important XMaS KPIs is the number and quality of publications. We ask you to provide Sophie Wawman with the reference and DOI whenever a new paper is published. Alternatively, you can submit your new publication reference directly through a form on our web site (**https://bit.ly/2Gja4zX**). Please also let us know about other impact generated as a result of XMaS work.

**IMPORTANT!**
It is important that we acknowledge the support from EPSRC in any publications. When beamline staff have made a significant contribution to your scientific investigation you may naturally want to include them as authors. Otherwise we ask that you add an acknowledgement of the form:

*"XMaS is a UK national research facility supported by EPSRC. We are grateful to all the beamline staff for their support."*

Editor: Laurence Bouchenoire - Graphic Designer: Sylvie Quercia - February 2025

XMaS the UK-CRG

**XMaS (BM28)**
**the UK Materials Science Beamline**

ESRF - The European Synchrotron
71 avenue des Martyrs, CS 40220
38043 Grenoble Cedex 9,
France

Tel: +33 (0)4.76.88.25.80
xmas@esrf.fr

@XMaSBeam

**www.xmas.ac.uk**

UNIVERSITY OF LIVERPOOL
UKRI Engineering and Physical Sciences Research Council
WARWICK THE UNIVERSITY OF WARWICK